Surface Science 679 (2019) 188–195

Contents lists available at ScienceDirect

Surface Science

journal homepage: www.elsevier.com/locate/susc

The nature of electrophilic oxygen: Insights from periodic density functional theory investigations

Nivedita Kenge[a], Sameer Pitale[a,b], Kavita Joshi[*,a,b]

[a] Physical and Materials Chemistry Division, CSIR-National Chemical Laboratory, Pune 411008 India
[b] Academy of Scientific and Innovative Research (AcSIR), Anusandhan Bhawan, 2, Rafi Marg, New Delhi 110001, India

ARTICLE INFO

Keywords:
Epoxidation
Ag(100)
DFT
Electrophilic
Nucleophilic oxygen

ABSTRACT

Increasing demand of ethylene oxide and the cost of versatile chemical ethene has been a driving force for understanding mechanism of epoxidation to develop highly selective catalytic process. Direct epoxidation is a proposed mechanism which in theory provides 100% selectivity. A key aspect of this mechanism is an electrophilic oxygen (O_{ele}) species forming on the Ag surface. In the past two and half decades, large number of theoretical and experimental investigations have tried to elucidate formation of O_{ele} on Ag surface with little success. Equipped with this rich literature on Ag-O interactions, we investigate the same using periodic DFT calculations to further understand how silver surface and oxygen interact with each other from a chemical standpoint. Based on energetics, Löwdin charges, topologies and *pdos* data described in this study, we scrutinize the established notions of O_{ele}. Our study provides no evidence in support of O_{ele} being an atomic species nor a diatomic molecular species. In fact, a triatomic molecular species described in this work bears multiple signatures which are very convincing evidence for considering it as the most sought for electrophilic entity.

1. Introduction

Silver catalyzed ethene (En) epoxidation by oxygen to produce ethylene oxide (EtO) is one of the most well-known kinetically controlled reaction in chemistry. It is also one of the most studied example in discipline of heterogeneous catalysis, owing to the great economic importance of EtO as well as En [1–3]. Ethene in presence of oxygen undergoes total combustion to CO_2 and H_2O virtually under all conditions except when the reaction is carried out in presence of Ag, where (for unpromoted Ag) the product is 50% EtO and rest are the combustion products [4]. From thermodynamic data, it is very clear that combustion products are far more stable owing to their reduced free energy. Even EtO, very rapidly decomposes into same combustion products due to its thermochemical instability. EtO can thus form only under conditions of kinetic control as it has low free energy of activation and not at conditions of thermodynamic equilibrium [5]. A kinetically controlled reaction involves reaction intermediate with low free energy of activation and is independent of free energy of formation of the product [6]. At present, 50% selectivity of bare Ag towards epoxidation is well understood through Oxometallacycle (OMC) intermediate based reaction mechanism proposed by Linic and Barteau [7]. Chief triumph of OMC mechanism is that it explains all the experimental observations not well understood over the decades. This includes proving the hypothesis of common intermediate for EtO and combustion products, [8] C–H bond breaking and proton transfer as rate limiting step for combustion, and excellent correlation to micro kinetic data [9–11]. Still OMC cannot explain ~ 90% selectivity of modern industrial catalysts [3,12]. In order to account for selectivity of industrial catalyst, it has been hypothesized that reaction under those conditions must go through direct epoxidation wherein an electrophilic oxygen (O_{ele}) species is formed on the promoted Ag surface under industrial reaction conditions [10]. EtO is thus formed as a result of an electrophilic attack on ethene through an addition reaction. Theoretically, such a mechanism has 100% selectivity for EtO and thus provides very lucrative basis for further improvement of industrial processes. Though theoretical aspects of direct epoxidation mechanism are fairly straight forward, [13] identity of O_{ele} has not been established unanimously to date. Nearly all the research on epoxidation in 21st century and most from the final decade of the last century is focused on characterization of O_{ele} [14–24]. And though considerable work has been already done in this field, the exact nature, electronic configuration or topological data about O_{ele} has remained controversial [23–25]. Until 2001, when Bukhtiyarov et al. published XANES, XPS, and UPS studies on Ag–O interactions, concluding O_{ele} has to be atomic in nature, whether O_{ele} is atomic or molecular was also the cause of considerable debate [14,17,18].

* Corresponding author at: Physical and Materials Chemistry Division, CSIR-National Chemical Laboratory, Pune 411008 India.
E-mail address: k.joshi@ncl.res.in (K. Joshi).

https://doi.org/10.1016/j.susc.2018.09.009
Received 9 August 2018; Received in revised form 10 September 2018; Accepted 15 September 2018
Available online 17 September 2018
0039-6028/

Density Functional Theory (DFT) based studies have proven themselves as indispensable tools for surface chemistry. OMC mechanism was also discovered through DFT studies [7]. Since then DFT based investigations of Ag–O interaction has become an attractive avenue for computational research. Through extensive computational studies carried out on multiple Ag facets, no species could be isolated which can fit the description of O_{ele} [17–24]. But in wealth of thermodynamic and physical data available through these studies, there seems to be glaring omission of chemical aspects of Ag–O interactions. Ag–O interactions are surprisingly diverse in nature and highly dependent of temperature, pressure as well as Ag facets and concentration of oxygen [20,26,27].

Oxidation of Ag surface to form bulk oxide like Ag_2O is a complicated process as observed in the recent studies [28–31]. Thin bulk oxide like Ag_2O layer formation shows reversible behavior with increase in temperature [28]. Recent experimental studies on Ag clusters supported on silica reveal that, larger clusters with 55 Ag atoms do not undergo complete oxidation [32]. Instead of forming stable Ag_2O phase, Ag prefers to maximize its coordination with O through interaction with molecular oxygen and this results in observed propensity of atomic O to occupy subsurface sites [30]. Further, O_2 chemisorption results in covalent interactions with Ag atoms [29]. Combined DFT and experimental investigations revealed that a low coverage of adsorbed atomic oxygen exists on Ag surface [33]. Further, studies carried out by Jones et al. concluded that O-1s signature of O_{ele} can only come from covalently bonded oxygen [24]. Additionally, authors noted that surface adsorbed atomic oxygen do not interact covalently enough to give rise to O_{ele} signatures in O-1s binding energies. They proposed that further research should focus on understanding how to make Ag–O interactions more covalent. In this light, recent publication on Ag–O interactions described the formation of SO_4 on the surface of Ag due to sulphurous impurities as a suspected source of O_{ele} [34].

It is worth noting here some industrial facts regarding epoxidation. For epoxidation process at an industrial scale, apart from Ag catalysts, high pressure (5–30 bar) and controlled temperature in the range of (423–623 K) are necessary conditions [12]. Though, the reported selectivities at industrial level are ~ 90%, Et to EtO conversion rates are typically low around 15% [12,35]. A recent experimental study based on temporal analysis at atmospheric pressure, of epoxidation products, demonstrates that conversion of Et to EtO never exceeded 20% at 44% selectivity typical for bare and unpromoted Ag [36]. Thus, high pressure, high oxygen concentration (compared to Et) in the feed and strict temperature control are unique characteristics of industrial scale ethene epoxidation apart from promoted catalytic surface.

To search for O_{ele} which is a key to direct epoxidation, we have modeled Ag–O interactions at various monolayer concentrations of O on Ag(100) surface. For an electrophilic oxygen to exist on Ag surface, it should have following two characteristic chemical features. Firstly, it should have a positive charge and secondly, it should be a covalently bonded species with empty states in the energy range 0–6 eV [24,37]. These empty states enable such species to accept electrons from ethene π orbitals. From our review of the literature, we could not find any work describing existence of such empty states. Therefore, we re-investigate Ag-O interactions to uncover the nature of bonding as well as configurations leading to O_{ele} signatures. Through exhaustive modeling of topologies using DFT, partial density of states (*pdos*) and Löwdin charge calculations we present a chemically intuitive picture of Ag-O interactions to seek answer for questions such as, what is the nature of Ag–O interactions? Are they predominantly ionic or covalent? Do electrophilic and nucleophilic oxygen form from Ag–O interactions alone? Is it possible to observe empty states for oxygen species chemisorbed on Ag surface? Could such species posses positive charge? We hope our efforts could provide some insight which can help in pursuit of elucidating the direct epoxidation mechanism.

Table 1
Relative energy (ΔE), Ag-O coordination along with bond length, and Löwdin charges on oxygen for different positions of oxygen at 0.25 ML coverage. The most stable structure has highly coordinated oxygen with maximum Löwdin charge.

Configuration description	ΔE (eV)	Ag-O coordination	Ag–O bond length Å	Löwdin charge on O
O_{4FH}	0.00	4	2.25	6.53
O_{2FB}	0.82	2	2.05	6.46
O_{1FT}	1.89	1	1.94	6.39

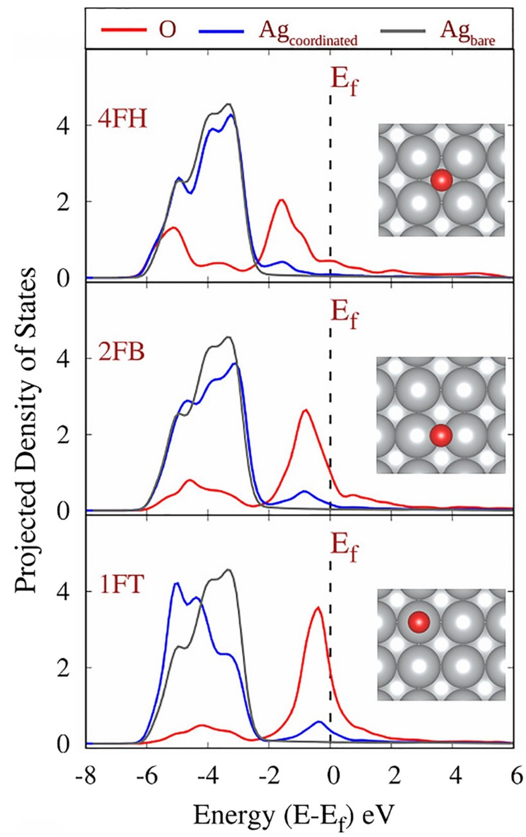

Fig. 1. Site dependent *pdos* for 4d-states of surface Ag atoms in bare slab (gray), 4d-states of surface Ag atoms coordinated with O (blue) and 2p-states of adsorbed O on Ag surface (red). Their respective configurations are also shown. 2p-states for four fold coordinated oxygen atom are the most delocalized among all the configurations. (For interpretation of the references to color in this figure legend, the reader is referred to the web version of this article.)

2. Computational details

We have investigated interaction of O with Ag(100) surface by employing Kohn-Sham formulation of DFT. The interaction between electrons and ions was modeled with Projector Augmented Wave pseudopotential with Perdew–Burke–Ernzerhof (PBE) exchange-correlation within generalized gradient approximation, as implemented in the plane wave code, Quantum ESPRESSO [38–42]. Energy cutoff for plane-waves was kept at 70 Ry and 700 Ry for charge density. The Ag surface was modeled by cleaving a surface with 4 layers in (100) direction. The vacuum along *z*-axis which is also (100) direction of the crystal was varied from 10 Å till 30 Å with the step of 2 Å. It was found that 20 Å of vacuum is sufficient to avoid interaction between adjacent images of planes along the *z*-direction. Since adsorption of reactant molecule/s on one side of slab gives rise to inhomogeneity in electric field, dipole field correction was applied in the *z*-direction in order to compensate this inhomogeneity. Geometry optimization was carried

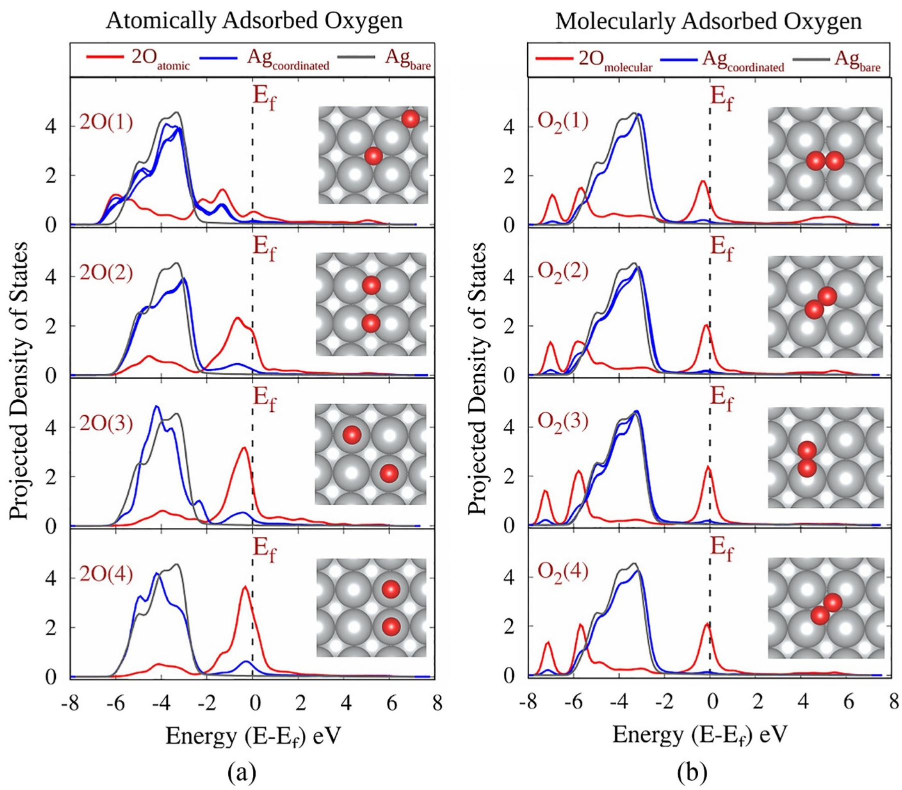

Fig. 2. Site dependent *pdos* for (a) atomically adsorbed oxygen (2O) and (b) molecularly adsorbed oxygen (O_2) on Ag(100) surface at 0.5 ML along with their respective configurations. Ag-4d states of bare slab are shown in gray, 4d states of coordinated Ag surface atoms are shown in blue and 2p states of oxygen are indicated in red color. *pdos* for atomically adsorbed oxygen shows striking similarity with that of single oxygen case discussed earlier. (For interpretation of the references to color in this figure legend, the reader is referred to the web version of this article.)

Table 2
Relative energy (ΔE), Ag–O coordination along with bond length, O-O bond lengths, and Löwdin charges on oxygen for various configurations of oxygen at 0.5 ML coverage. Atomically adsorbed configurations (2O(1) to 2O(4)) are shown in red color and molecularly adsorbed configurations are indicated in (O_2(1) to O_2(4)) in green color..

Sr. no.	Configuration description	ΔE (eV)	Ag-O coordination	Ag-O bond length(Å)	O-O bond length(Å)	Löwdin charge on O
1.	2O(1)	0.00	4	2.11-2.21	-	6.49
2.	O_2(1)	0.73	2	2.26	1.42	6.52
3.	O_2(2)	1.16	2	2.27-2.41	1.37	6.18
4.	O_2(3)	1.17	1	2.22	1.31	6.09
5.	O_2(4)	1.18	1	2.26	1.36	6.17
6.	2O(2)	2.08	2	2.04	-	6.35
7.	2O(3)	3.62	1	1.97	-	6.43
8.	2O(4)	4.32	1	1.97	-	6.28

out with a force cutoff of 10^{-3} a.u. on the unfixed atoms and the total energies were converged below 10^{-4} a.u. A Monkhorst-Pack grid of 12x12x1 was used which resulted into 72 k-points in IBZ to emulate the solid slab.

As we focused on silver–oxygen interaction, the system was chosen in such a way that it can be exhaustively studied at optimal computational expenses. In a 2X2 slab, based on symmetry arguments, three distinct surface sites exist. Also the calculations are carried out under periodic boundary conditions and thus the system can be repeated infinitely to model macroscopic surface. But as unit cell for such macroscopic model consists of surface created by four Ag atoms, inclusion of single oxygen atom on surface is equivalent to 1/4 monolayer (ML) coverage of oxygen which is equivalent to the model of pristine silver surface coated with 1/4 ML of oxygen under experimental conditions. Under these circumstances, our model enables us to study 0.25 ML (one oxygen), 0.5 ML (two oxygen atoms), 0.75 ML (three oxygen atoms) and 1 ML (four oxygen atoms). As attaining 1 ML is very difficult under experimental conditions and adding four atoms in such a small system results in severe distortions, we have not included cases of the same in this study. We have considered all possible configurations under 0.25, 0.5, 0.75 monolayers, where oxygen atom or molecule can occupy unique positions. Thus, it is ensured that all types of silver-oxygen bonding configurations are investigated. A small modeled system has obvious disadvantages when it comes to elucidation of reaction intermediates and mechanisms. However, we have defined the goal of this study, to investigate adsorption of oxygen on silver and to understand the nature of bonding in such interactions. Hence, this small system provides a modest starting point. In the following section, we discuss the interaction between O species and Ag(100) surface as a function of increasing concentration of O. As noted earlier, the surface was modeled by considering four layers of Ag(100) with 2x2 supercell. The bottom most layer is fixed. Thus, our simulation box contains 16 Ag atoms. Number of oxygen atoms varies based on the monolayer concentration of O.

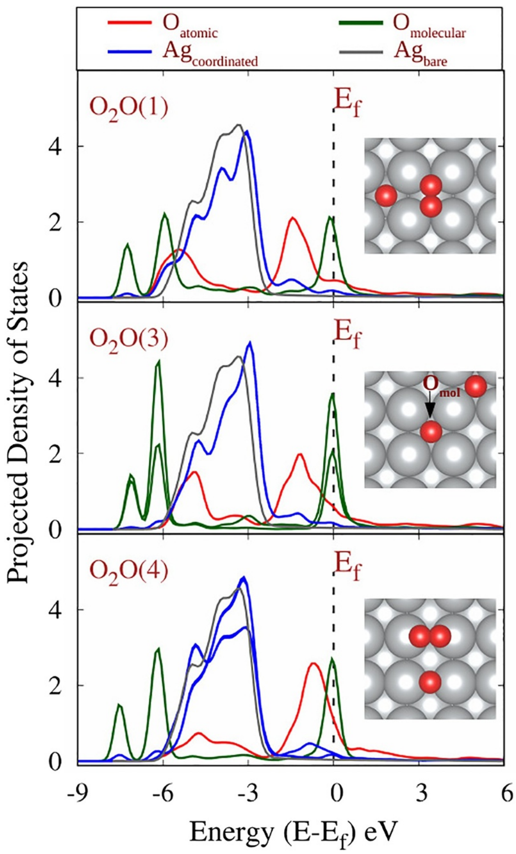

Fig. 3. Site specific *pdos* of O_2O configurations at 0.75 ml along with their respective configurations. 2p states of O_2 are shown in green and 2p states of atomic O are shown in red color. The pdos for combined atomic and molecularly adsorbed oxygen resembles chemical features of configurations at 0.25 ml and molecular configurations at 0.5 ml. (For interpretation of the references to color in this figure legend, the reader is referred to the web version of this article.)

3. Results and discussion

In this section, we take a closer look in the chemical signatures and trends generated therein to relate the data with observations made both experimentally and theoretically in prior literature. The focus of this discussion is to bring out probable configurations which will support existence of electrophilic oxygen species which leads to direct epoxidation. For the case of 0.25 ML, we have studied interactions of oxygen with Ag surface at three distinct surface sites such as 4 fold hollow (4FH), 2 fold bridge (2FB), and 1 fold top (1FT). Details regarding the energetics, Ag–O bond lengths as well as coordination, and Löwdin charges of oxygen atom are summarized in Table 1. The configurations along with site dependent *pdos* are shown in Fig. 1. Out of these three surface configurations, oxygen adsorbed at hollow site (4FH) is energetically the most preffered configuration followed by the bridge position (2FB) and the least stable is on-top site (1FT). Ag-O bond length increases with coordination and is noted in Table 1. Löwdin charge analysis manifests that charge of higher coordinated oxygen species is greater in magnitude while for lower coordinated oxygen atom, magnitude of charge is lesser. Site dependent *pdos* brings out interesting observations related to the site specific interaction between surface Ag atoms and adsorbed oxygen as shown in Fig. 1. The *pdos* for O-2*p* associated with on-top oxygen peaks near Fermi level (E_f) and it is relatively sharper. On the other hand, the peak position of O-2*p* shifts away from E_f and is accompanied with broadening of peaks as coordination of adsorbed oxygen increases for 2FB and 4FH configurations. When considering 2*p*-4*d* overlap, a sharp peak in *pdos* represents localized electron distribution and thus ionic character of the bond. Conversely, broader peak suggests delocalized state and alludes to covalent character of the bond [43].

Surface Ag–O interactions, modeled on the basis of Ag_2O in previous investigations, considered it to be ionic in nature [44]. Contrary to this, our studies bring out that surface Ag–O interactions are preferably covalent in nature with little tendency towards formation of Ag_2O. This preferred covalent bonding is unique for Ag among other transition metals where oxidation of surface and formation of ions is a norm. Because of high energetic cost of ion formation, covalent overlap with multiple states seems to be preferred mode of bonding for oxygen on Ag surface. This explains, why hollow position is a preferred site over bridge and top positions. Another important observation provided by *pdos* is a lack of empty states near E_f. Availability of these states near E_f is an essential criterion for reaction to occur. As none of the atomic oxygen species possess any compatible states above E_f for accepting π-electrons from ethene, we conclude that single atomic oxygen species should be precluded as contributing factor in the direct epoxidation. Considering 0.5 ML coverage, all the configurations tested can be classified into two groups, viz. atomically adsorbed oxygen atoms (2O) distributed over three distinct sites and molecularly adsorbed oxygen (O_2) placed at various sites. Adsorption of two atomic oxygen leads to eight initial configurations and adsorption of molecular oxygen leads to five initial configurations. These thirteen initial configurations resulted into eight stable configurations upon relaxation and are shown in Fig. 2 along with their site dependent *pdos*. Cases in which two oxygen atoms are more than 2 Å apart are considered as atomically adsorbed. For these eight stable configurations, relative energies, Ag-O coordination, Ag–O and O–O bond lengths, and Löwdin charges are summarized in Table 2 where 2O configurations are shown in red color and O_2 configurations are shown in green.

Although, energetically the most stable configuration is the adsorption of two atomic oxygen at hollow site, it is followed by four configurations where adsorbed oxygen is in molecular form. Interestingly, among these molecularly adsorbed O_2 configurations, O–O bond is the weakest in O_2(1). This signifies importance of Ag–O coordination even for molecularly adsorbed oxygen.

pdos along with the configuration for atomically adsorbed oxygens is shown in Fig. 2(a) where as configurations with molecularly adsorbed oxygen are shown in Fig 2(b). As seen in Fig. 2(a), *pdos* for atomic cases are strikingly similar to their counterparts in 1O scenario. Hence, discussion in this section will focus on the molecularly adsorbed oxygen. In case of molecularly adsorbed oxygen, *pdos* for all the cases are very similar, exhibiting signature of molecular oxygen which is considerably different than that of atomically adsorbed oxygen. Further, the most stable molecularly adsorbed oxygen also exhibit more delocalisation among this class. As established for 1O cases, increase in overall delocalisation between O-2p and Ag-4d states indicates increasing stability of the configuration. Similarly, molecular structure with maximum potential for electron delocalisation turns out to be the most stable as seen in case of O_2 at hollow (O_2(1)) and as emphasized in O_2 across corner Ag (O_2(2)), where at the cost of steric crowding better Ag–O and O–O bonding is achieved. This emphasizes nature of Ag-O interactions which do not favor formation of well defined molecules but weakly bonded moieties with maximum possible coordination for each atom involved. Löwdin charges preclude consideration of any oxygen species studied here as an electrophile from ionic standpoint. Further, lack of empty states near E_f emphasis their inability to accept π electrons from ethene. Thus, these configurations cannot be considered as electrophiles from covalent standpoint also. Owing to this analysis, such dissociatively adsorbed diatomic molecular oxygen species should be precluded as contributing factor in direct epoxidation.

In case of 0.75 ML, we have modeled the system by adsorbing three atomic oxygen (3O), combination of atomic and diatomic molecular oxygen (O_2O) and triatomic molecular oxygen (O_3) to account for all possible combinations. We would like to emphasis that O_3 is different

Table 3
Relative energy (ΔE), Ag–O coordination along with bond length, and Löwdin charges on oxygen for different positions of oxygen at 0.75 ML coverage. Configurations like combination of atomic and molecular O are shown in blue (O_2O(1) to O_2O(5)) and triatomic molecular configurations (O_3(1) to O_3(7) in green color.

Sr. no.	Configuration description	ΔE (eV)	Ag-O coordination	Ag-O bond length(Å)	O-O bond length(Å)	Löwdin charge on O
1.	$O_2O(1)$	0.000	O_2=2	2.38	1.33	O_2=6.08
			O=4	2.21	-	O=6.50
2.	$O_2O(2)$	0.043	O_2=2	2.35	1.35	O_2=6.11
			O=4	-	2.22	O=6.48
3.	$O_3(1)$	0.083	O_{End}=2	2.28	1.39	O_{End}=6.22
			O_{Mid}=0	-	-	$\boxed{O_{Mid}=5.85}$
4.	$O_3(2)$	0.229	O_{End}=2	2.27-2.42	1.37	O_{End}=6.22
			O_{Mid}=0	-	-	$\boxed{O_{Mid}=5.82}$
5.	$O_2O(3)$	0.306	O_2=0	-	1.28	O_2=6.03
			O=4	2.23	-	O=6.50
6.	$O_3(3)$	0.340	O_{End1}=2	2.29	1.32-1.47	O_{End1}=6.27
			O_{End2}=1	2.40	-	O_{End2}=6.16
			O_{Mid}=0	-	-	$\boxed{O_{Mid}=5.83}$
7.	$O_3(4)$	0.343	O_{End1}=3	2.39-2.43	1.32-1.48	O_{End1}=6.28
			O_{End2}=1	2.30	-	O_{End2}=6.16
			O_{Mid}=0	-	-	$\boxed{O_{Mid}=5.83}$
8.	$O_3(5)$	0.548	O_{End}=1	2.24	1.34	O_{End}=6.19
			O_{Mid}=0	-	-	$\boxed{O_{Mid}=5.75}$
9.	$O_3(6)$	0.558	O_{End}=1	2.24	1.34	O_{End}=6.17
			O_{Mid}=0	-	-	$\boxed{O_{Mid}=5.73}$
10.	$O_2O(4)$	1.010	O_2=1	2.28	1.27	$\boxed{O_2=5.98}$
			O=2	2.03	-	O=6.43
11.	$O_2O(5)$	1.070	O_2=1	2.31	1.28	$\boxed{O_2=5.99}$
			O=2	2.04	-	O=6.42
12.	$O_3(7)$	1.441	O_{End}=1	2.43	1.36	O_{End}=6.20
			O_{Mid}=0	-	-	$\boxed{O_{Mid}=5.77}$

than molecular allotropic ozone. In this work, we refer triatomic oxygen species as O_3 and allotrope as ozone. Three atomic oxygens lead to twelve initial configurations, combination of atomic and diatomic molecular oxygen leads to eighteen initial configurations, and triatomic molecular oxygen lead to six initial configurations. All these thirty six initial configurations resulted into twelve stable configurations upon relaxation. These configurations are classified into two groups viz., five configurations of O_2O and seven configurations of O_3. Fig. 3 represents three distinct configurations out of five.[1] Energetics, Ag–O and O–O coordination, Ag–O and O–O bond lengths, and Löwdin charges on oxygen of all relaxed configurations are summarized in Table 3 where O_2O cases are shown in blue color and O_3 cases are shown in green color for a clear distinction. Configurations which show positive charge on oxygen are highlighted.

The configuration (O_2O(1)) in which both atomic and molecular oxygen adsorbed at hollow site has the lowest energy. However, if we consider ten most stable configurations they are dominated by adsorption of triatomic molecular oxygen as evident from Table 3 Keen observation of Fig. 3 reveals that *pdos* of O_2O configurations coincide with combined *pdos* of atomic O (shown in Fig. 1) and molecularly adsorbed oxygen (shown in Fig. 2). This suggests that, these entities do not affect the chemical nature of each other. Löwdin charges on oxygen for O_2O(4) and O_2O(5) show marginal positive charge; but empty states which are indispensable for direct epoxidation are not present beyond E_f in nearby locus. Thus, we precluded these configurations as candidates for electrophilic oxygen.

Fig. 4 represents top and side view of six out of seven O_3 configurations along with their respective *pdos*.[2] Adsorption of three oxygen as O_3 on Ag surface leads to end oxygens coordinating with Ag. As Table 3 suggests that middle oxygen(O_{mid}) of all O_3 configurations possess significant positive charge (highlighted in Table 3). Further, as seen in Fig. 4 all these configurations with adsorbed O_3 show presence of empty states beyond E_f in energy range $3.5 - 5.5$ eV which is a characteristic feature of electron deficient species.

If direct epoxidation by means of electrophilic attack of oxygen on

[1] Two configurations (O_2O(2) and O_2O(5)) are not included on the basis of their similar *pdos* nature.

[2] The one with similar *pdos* is not included.

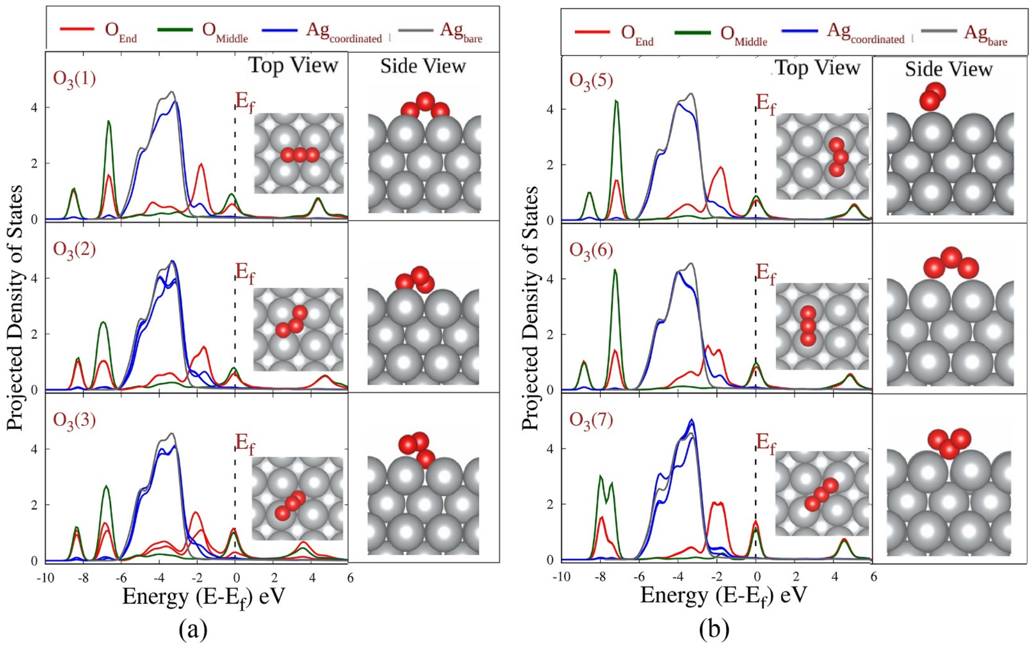

Fig. 4. Site specific *pdos* for O_3 configurations at 0.75 ml along with top and side view of stable configurations. 2p states of O_{mid} are shown in green and 2p states of O_{end} atoms are shown in red. Availability of empty states near E_f are observed in all the configurations. (For interpretation of the references to color in this figure legend, the reader is referred to the web version of this article.)

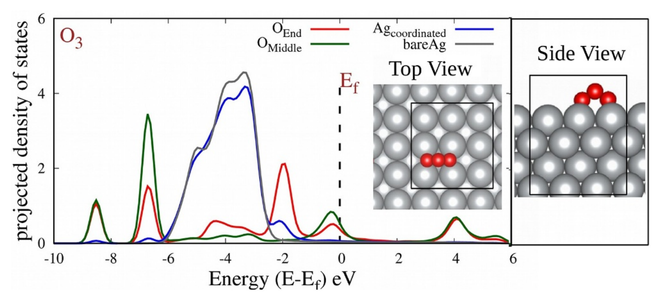

Fig. 5. Site specific *pdos* for O_3 configuration on a 3x3 supercell along with top and side view of the configuration. 2p states of O_{mid} are shown in green and 2p states of O_{end} atoms are shown in red. Availability of empty states near E_f are observed demonstrating that it is not an artifact of a smaller slab. (For interpretation of the references to color in this figure legend, the reader is referred to the web version of this article.)

ethene is the main mode of industrial epoxidation then such O_{ele} must feature characteristics of an electrophile. In case of ethene which has π orbitals at E_f and π* orbital at 6 eV, O_{ele} must possess empty states matching energy range of ethene π [37]. This will facilitate overlap among these orbitals into which π electrons can be transferred. In case of O_3 species, this could be further facilitated by positive charge on middle oxygen. Again presence of weak O–O bonds in this species will further help dissociation of middle oxygen from O_3 moiety. Also, a notable fact is that this state arises out of O-2p interactions alone and have no contribution from Ag-4d or Ag-5s orbitals, this is contradictory to the presumption that O_{ele} must have significant overlap with Ag-4d or Ag-5s [15,24,45].

To demonstrate that O_3 is not an artifact of a smaller slab that has been modeled here, we have also computed *pdos* of O_3 on a larger supercell. Fig. 5 shows the site dependent *pdos* for O_3 on a 3x3 supercell. O_3 exhibits similar features in *pdos* demonstrating that indeed middle oxygen in O_3 moiety bares signatures of electrophilic oxygen. The Löwdin charge on the middle oxygen is 5.896. Thus it fulfills both the conditions of an electrophile.

However, prevalence of the O_3 will be much more at elevated pressures. To demonstrate this we have also optimized a 5x5 supercell at 1 ML coverage. The initial configuration along with optimized structure are shown in Fig 6. The initial configuration (see Fig. 6-a) consists of sixteen oxygen atoms at hollow positions and nine oxygen atoms at on top positions resulting into 1 ML coverage. The relaxed structure is shown in Fig. 6-b. Different oxygen moieties are shown in different colors to aid an eye. This also brings out the complexity of the problem at hand. The optimized structure consists of three O_3 moieties, two O_2 molecules with extended O–O bondlength. There are few

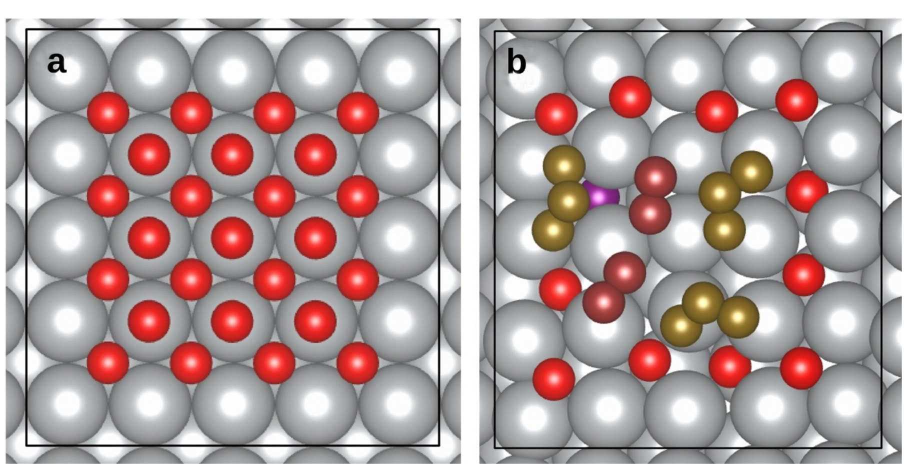

Fig. 6. For 5X5 Ag 100 surface shown in a box adsorbed with 25 oxygen a) initial configuration (top view) in which 16 oxygens placed at 4FH and 9 oxygens are at 1FT positions, b) final configuration (top view) shows presence off our types of oxygens viz,. atomic oxygen on the surface O (red), diatomic molecular oxygen O_2 (brown) and triatomic molecular oxygen O_3 (golden rod). The oxygen atom escalated to subsurface site is shown in purple color. The surface reconstruction is also evident from the figure. The 2x2 slab could not account for such surface reconstruction. (For interpretation of the references to color in this figure legend, the reader is referred to the web version of this article.)

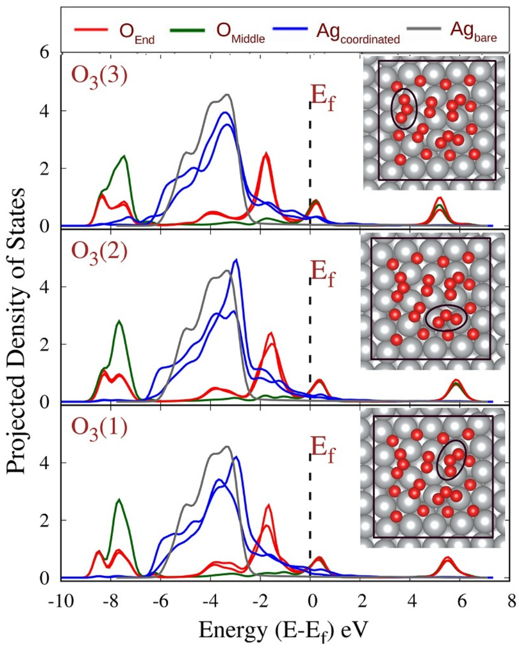

Fig. 7. Site specific *pdos* for O_3 configurations on a 5x5 supercell along with top and side view of the configurations. 2p states of O_{mid} are shown in green and 2p states of O_{end} atoms are shown in red. Availability of empty states near E_f confirms that O_{mid} is electrophilic in nature. (For interpretation of the references to color in this figure legend, the reader is referred to the web version of this article.)

oxygen atoms at hollow sites as well as few oxygen atoms have escalated to subsurface site. The figure also brings out the extensive surface reconstruction that took place upon relaxation. A point to be noted here is limitation of our 2x2 slab to bring out such surface reconstructions. However, the most important feature is all O_3 moieties observed in this structure bare both signatures of electrophilic oxygen. Only three middle oxygens in the three O_3 moieties have partially positive Löwdin charge. Rest of all oxygens are partially negatively charged although the magnitude of the charge varies based on their actual position. Further, the site dependent *pdos* for all the O_3 moieties (shown in Fig. 7) exhibit empty states above E_f. The *pdos* for O_2 and oxygen at hollow position are also similar to what we have shown in our 2x2 model except minor modifications due to surface reconstructions.

Thus, our simulations convincingly brings out signatures of electrophilic oxygen and scenario where this moiety will be present. At this point, an important question should be asked is, then why it was not detected so far? As our investigations show, O_3 will be more probable at higher pressures as well as temperatures. Although, the industrial catalyst for EtO works at higher pressure and temperature, most of the surface science studies are carried out at low pressures or very low pressures. And there is a pressure gap between the surface science experiments and working conditions of an industrial catalyst. We believe this is the most probable reason for not so successful search for the electrophilic oxygen. Few caveats should be noted when we are closing our discussions. First, scope of this work is limited, i.e. to search for the electrophilic oxygen. The formation of EtO on Ag surfaces have many aspects which are not being touched upon in this work and there are many open questions still exist and awaits explanations.

4. Conclusions

Ethylene epoxidation is one of the most investigated reactions in heterogeneous catalysis. Two types of oxygen species, electrophilic and nucleophilic oxygen were envisaged. Although, many experiments and simulations could bring out signatures of nucleophilic oxygen, so far electrophilic oxygen remains a mystery. In the present work, we investigate interaction between Ag(100) surface and oxygen as a function of monolayer concentration. Our extensive investigations reveal that at 0.25 ML and 0.5 ML the two signatures associated with electrophilic oxygen species viz. positive charge on oxygen and empty states near Fermi level are missing and so we can not consider these atomically or molecularly adsorbed oxygen as an electrophilic oxygen required for direct epoxidation. On the other hand, adsorbed O_3 species at 0.75 ML concentration bares signatures relevant for electrophilic oxygen. Middle oxygen in *all* adsorbed O_3 have significant positive charge as evident from their Löwdin charges as well as *all* these configurations have empty states in between 3.5 and 5.5 eV required to accept π electrons from ethene to form EtO. Thus, our investigations bring out situations corresponding to electrophilic oxygen required for direct epoxidation.

Acknowledgment

We are thankful to Dr. C. S. Gopinath for many fruitful discussions. CSIR-4PI is gratefully acknowledged for the computational facility. KJ and NK acknowledge DST (EMR/2016/000591) for partial financial support. SP acknowledges CSIR for research fellowship.

References

[1] W.M.H. Sachtler, C. Backx, R.A. Van Santen, Cataly. Rev. 23 (1–2) (1981) 127–149, https://doi.org/10.1080/03602458108068072.
[2] P. Dutia, Chem. Wkl. 55 (2010) 199–204.
[3] M.O. Özbek, R.A. van Santen, Catal. Lett. 143 (2) (2013) 131–141, https://doi.org/10.1007/s10562-012-0957-3.
[4] L.T. Emile, Process for the Production of Ethylene Oxide, 1935.
[5] H. Worbs, Dissertation, Technische Hochschule, Breslau; U.S. Office of Technical Service P.B. Rept. 98705., 1942 Ph.D. thesis.
[6] Smith, March, March's Advanced Organic Chemistry, Wiley, 2007.
[7] S. Linic, M.A. Barteau, J. Am. Chem. Soc. 124 (2) (2002) 310–317, https://doi.org/10.1021/ja0118136. PMID: 11782183
[8] E.L. Force, A.T. Bell, J. Catal. 40 (1975) 356–371, https://doi.org/10.1016/0021-9517(75)90267-5.
[9] C. Backx, J. Catal. 72 (2) (1981) 364–368, https://doi.org/10.1016/0021-9517(81)90019-1.
[10] R.V. Santen, H. Kuipers, Adv. Catal. 35 (1987) 265–321, https://doi.org/10.1016/S0360-0564(08)60095-4.
[11] S. Linic, M. Barteau, J. Catal. 214 (2) (2003) 200–212, https://doi.org/10.1016/S0021-9517(02)00156-2.
[12] Zakzeski, Catalyst for the Epoxidation of Alkenes, 2017.
[13] G.H. Twigg, Trans. Faraday Soc. 42 (1946) 284–290, https://doi.org/10.1039/TF9464200284.
[14] V.I. Avdeev, A.I. Boronin, S.V. Koscheev, G.M. Zhidomirov, J. Mol. Catal. A: Chem. 154 (1) (2000) 257–270, https://doi.org/10.1016/S1381-1169(99)00395-7.
[15] X. Bao, M. Muhler, T. Schedel-Niedrig, R. Schlögl, Phys. Rev. B 54 (1996) 2249–2262, https://doi.org/10.1103/PhysRevB.54.2249.
[16] V. Bukhtiyarov, V. Kaichev, J. Mol. Catal. A: Chem. 158 (1) (2000) 167–172, https://doi.org/10.1016/S1381-1169(00)00062-5.
[17] V. Bukhtiyarov, M. Hävecker, V. Kaichev, A. Knop-Gericke, R. Mayer, R. Schlögl, Catal. Lett. 74 (3) (2001) 121–125, https://doi.org/10.1023/A:1016666021405.
[18] W.-X. Li, C. Stampfl, M. Scheffler, Phys. Rev. B 65 (2002) 075407, https://doi.org/10.1103/PhysRevB.65.075407.
[19] V.V. Kaichev, V.I. Bukhtiyarov, M. Hävecker, A. Knop-Gercke, R.W. Mayer, R. Schlögl, Kinet. Catal. 44 (3) (2003) 432–440, https://doi.org/10.1023/A:1024459305551.
[20] J. Schnadt, J. Knudsen, X.L. Hu, A. Michaelides, R.T. Vang, K. Reuter, Z. Li, E. Lægsgaard, M. Scheffler, F. Besenbacher, Phys. Rev. B 80 (7) (2009), https://doi.org/10.1103/PhysRevB.80.075424.
[21] M.F. Fellah, R.A. van Santen, I. Onal, Catal. Lett. 141 (6) (2011) 762–771, https://doi.org/10.1007/s10562-011-0614-2.
[22] T.C.R. Rocha, A. Oestereich, D.V. Demidov, M. Hävecker, S. Zafeiratos, G. Weinberg, V.I. Bukhtiyarov, A. Knop-Gericke, R. Schlögl, Phys. Chem. Chem. Phys. 14 (13) (2012) 4554, https://doi.org/10.1039/c2cp22472k.
[23] S. Böcklein, S. Günther, J. Wintterlin, Angew. Chem. Int. Ed. 52 (21) (2013) 5518–5521, https://doi.org/10.1002/anie.201210209.
[24] T.E. Jones, T.C.R. Rocha, A. Knop-Gericke, C. Stampfl, R. Schlögl, S. Piccinin, ACS Catal. 5 (10) (2015) 5846–5850, https://doi.org/10.1021/acscatal.5b01543.
[25] N.M. Martin, S. Klacar, H. Grönbeck, J. Knudsen, J. Schnadt, S. Blomberg, J. Gustafson, E. Lundgren, J. Phys. Chem. C 118 (28) (2014) 15324–15331, https://doi.org/10.1021/jp504387p.
[26] M.-L. Bocquet, A. Michaelides, D. Loffreda, P. Sautet, A. Alavi, D.A. King, J. Am. Chem. Soc. 125 (19) (2003) 5620–5621, https://doi.org/10.1021/ja0297741. PMID: 12733886
[27] J. Derouin, R.G. Farber, M.E. Turano, E.V. Iski, D.R. Killelea, ACS Catal. 6 (7)

(2016) 4640–4646, https://doi.org/10.1021/acscatal.6b01239.
[28] M.K. Ghosalya, K.P. Reddy, R. Jain, K. Roy, C.S. Gopinath, J. Chem. Sci. 130 (3) (2018) 30, https://doi.org/10.1007/s12039-018-1434-3.
[29] M. Mehlhorn, K. Morgenstern, J Chem Phys 144 (13) (2016) 134706, https://doi.org/10.1063/1.4945339.
[30] S.B. Isbill, S. Roy, D.J. Keffer, Mol. Simul. 43 (5–6) (2017) 355–369, https://doi.org/10.1080/08927022.2016.1268258.
[31] M.M. Montemore, M.A. van Spronsen, R.J. Madix, C.M. Friend, Chem. Rev. 118 (5) (2018) 2816–2862, https://doi.org/10.1021/acs.chemrev.7b00217.
[32] T. Lünskens, C.A. Walenta, P. Heister, A. Kartouzian, U. Heiz, J. Cluster Sci. 28 (6) (2017) 3185–3192, https://doi.org/10.1007/s10876-017-1285-y.
[33] E.A. Carbonio, T.C.R. Rocha, A.Y. Klyushin, I. Píš, E. Magnano, S. Nappini, S. Piccinin, A. Knop-Gericke, R. Schlögl, T.E. Jones, Chem. Sci. 9 (2018) 990–998, https://doi.org/10.1039/C7SC04728B.
[34] T.E. Jones, R. Wyrwich, S. Böcklein, E.A. Carbonio, M.T. Greiner, A.Y. Klyushin, W. Moritz, A. Locatelli, T.O. Menteş, M.A. Niño, A. Knop-Gericke, R. Schlögl, S. Günther, J. Wintterlin, S. Piccinin, ACS Catal. 8 (5) (2018) 3844–3852, https://doi.org/10.1021/acscatal.8b00660.
[35] H. Kestenbaum, A. Lange de Oliveira, W. Schmidt, F. Schüth, W. Ehrfeld, K. Gebauer, H. Löwe, T. Richter, D. Lebiedz, I. Untiedt, H. Züchner, Ind. Eng. Chem. Res. 41 (4) (2002) 710–719, https://doi.org/10.1021/ie010306u.
[36] S. Ludwig, H. Raimund, Chem. Ing. Tech. 89 (10) (2017) 1350–1359, https://doi.org/10.1002/cite.201700071.
[37] A. Kokalj, A. Dal Corso, S. de Gironcoli, S. Baroni, Surf. Sci. 507 (2002) 62–68, https://doi.org/10.1016/S0039-6028(02)01176-7.
[38] P.E. Blöchl, Phys. Rev. B 50 (1994) 17953, https://doi.org/10.1103/PhysRevB.50.17953.
[39] G. Kresse, D. Joubert, Phys. Rev. B 59 (1999) 1758, https://doi.org/10.1103/PhysRevB.59.1758.
[40] J.P. Perdew, K. Burke, M. Ernzerhof, Phys. Rev. Lett. 77 (1996) 3865, https://doi.org/10.1103/PhysRevLett.77.3865.
[41] J.P. Perdew, K. Burke, M. Ernzerhof, Phys. Rev. Lett. 78 (1997) 1396, https://doi.org/10.1103/PhysRevLett.78.1396.
[42] P. Giannozzi, S. Baroni, N. Bonini, M. Calandra, R. Car, C. Cavazzoni, D. Ceresoli, G.L. Chiarotti, M. Cococcioni, I. Dabo, A. Dal Corso, S. de Gironcoli, S. Fabris, G. Fratesi, R. Gebauer, U. Gerstmann, C. Gougoussis, A. Kokalj, M. Lazzeri, L. Martin-Samos, N. Marzari, F. Mauri, R. Mazzarello, S. Paolini, A. Pasquarello, L. Paulatto, C. Sbraccia, S. Scandolo, G. Sclauzero, A.P. Seitsonen, A. Smogunov, P. Umari, R.M. Wentzcovitch, J. Phys.: Condens. Matter 21 (39) (2009). 395502 (19pp)
[43] R. Hoffmann, Angew. Chem. Int. Ed. Engl. 26 (9) (1987) 846–878, https://doi.org/10.1002/anie.198708461.
[44] V.I. Bukhtiyarov, A.I. Nizovskii, H. Bluhm, M. Hävecker, E. Kleimenov, A. Knop-Gericke, R. Schlögl, J. Catal. 238 (2) (2006) 260–269, https://doi.org/10.1016/j.jcat.2005.11.043.
[45] V. Bukhtiyarov, M. Hävecker, V. Kaichev, A. Knop-Gericke, R. Mayer, R. Schlögl, Catal. Lett. 74 (3) (2001) 121–125, https://doi.org/10.1023/A:1016666021405.